Comprehensive Imager Simulation for Improved Acoustic Power Control

Chris M.W. Daft, William M. Leue, Kai E. Thomenius,
Michael C. Macdonald and Lars A. Ødegaard.

Abstract— **Commercial ultrasound imagers must comply with the FDA 510(k) regulations to be marketed in the USA. Controlling the acoustic output to meet these requirements is complex. There are hundreds of thousands of discrete operating conditions available to the sonographer. Accurate measurements require "peaking" of the hydrophone in azimuth and elevation, and acquiring data as a function of range. The acoustic field needs to be characterized in 3 dimensions. It is impossible to measure the imager's output under each condition, so algorithmic means are needed to reduce the size of the problem. Even when simple linear dependencies (such as pulse repetition frequency) are taken into account, the time to obtain Thermal and Mechanical Indices for a new probe is formidable. We also must repeat the experiment each time changes are made to the transmitter hardware, or its waveforms. We present further results on how to speed the acquisition of data used for estimation of the output labeling parameters by guiding the water-tank measurements with a beam simulator. The linear simulation uses the *FIELD II* code from the Technical University of Denmark [1]. The advantages and limitations of such an approach are detailed with reference to bracketing the maximum power search range. We also give an assessment of the reliability of the simulated values in view of nonlinear ultrasound propagation. Nonlinear effects are especially difficult to simulate since water offers little attenuation to the harmonics generated during propagation. Quite frequently, this nonlinearity is sufficient to redistribute the peak positions of the various acoustic intensities.**

Keywords— **ultrasound imaging, acoustic power, nonlinearity, 510(k), simulation, exposimetry, output display standard, bioeffects.**

I. INTRODUCTION

The acoustic output of commercial ultrasound scanners is regulated in the USA by the Food and Drug Administration (FDA) using a measurement standard defined by the National Electrical Manufacturers' Association (NEMA) [2]. Somewhat similar measurements are required by the IEC in Europe. In the early 1990s, the American Institute of Ultrasound in Medicine (AIUM), NEMA and several clinical organizations collaborated to develop the Output Display Standard (ODS), a standard governing the display of on-screen acoustic power parameters. These indices provide the physician with information on the probability of bioeffects. The Thermal Index (*TI*) is an estimate of the maximum tissue temperature rise for a given acoustic output level, in steady-state conditions. It is generally proportional to the time integral of the squared pressure. The Mechanical Index (*MI*) is intended to gauge the likelihood of nonthermal bioeffects, and is computed from the derated peak rarefactional pressure $P_{r.3}$ (in MPa) as:

$$\mathrm{MI} = \frac{P_{r.3}(z_{SP})}{\sqrt{f_c}} \qquad (1)$$

where f_c is the center frequency of the pulse in MHz, and z_{SP} is the range at which the pulse intensity integral PII.3 reaches its maximum. The requirements that a manufacturer must meet are twofold:

- The derated $I_{\mathrm{SPTA.3}}$ (spatial peak, temporal average intensity) and MI (as well as the other indices TIS, TIB and TIC) are to be within the values specified by the FDA. For Track 3 machines (those with output display), $I_{\mathrm{SPTA.3}}$ must not exceed 720 $\mathrm{mWcm^{-2}}$ and MI should be less than 1.9. A statistical definition of this limit is given in terms of production sampling, which encourages accurate measurement. That is, the better we have the acoustic power controlled, (in terms of machine-to-machine and probe-to-probe variation) the higher the mean acoustic output can be. Higher acoustic power values produce better image quality deep in the patient.
- A meaningful display of MI, TIS, TIB and TIC is required for all modes.

These measurements are technically challenging in themselves; also, the vast number of discrete operating conditions of a modern scanner precludes comprehensive measurement. Sandstrom [3] cites the ATL HDI-5000 machine as having 100,000 conditions per probe, and our experience is that this number can easily increase. In part, this huge value comes from striving to provide the clinician with better image quality, and more preset settings appropriate for different applications.

Compounding the problem is the effect of nonlinear sound propagation in water. In many imager settings, nonlinear propagation must be considered; this complicates assessment of bioeffects since the MI and TI were conceived in a linear regime. For example, the pressure used for the MI may be far from the focus at high output levels [4]. In tissue, harmonics are generated, but the higher harmonics attenuate quickly, and a balance between absorption and generation is reached with only moderate waveform distortion. Regulatory measurements are made in water, and then derated by 0.3 $\mathrm{dB\,cm^{-1}MHz^{-1}}$. The low attenuation of water (compared to tissue) makes simulation of sound propagation difficult in view of the large number of harmonics generated. Madsen *et al.* [5] have proposed a tissue mimicking liquid to replace *derated water* in these measurements to improve their predictive value. Using such a medium would also be easier to measure and simulate.

CMWD [daft@ieee.org], WML and KET are with GE Corporate R&D, Schenectady, NY, USA.
MCM is with GE Medical Systems, Milwaukee, WI, USA.
LAO is with GE Vingmed, Horten, Norway.

0-7803-5722-1/99/$10.00

The measurement speed for each discrete operating condition is determined by several factors, including:

- Lateral and radial search range
- Lateral and radial sampling density
- Propagation time in water
- Data transfer rate from oscilloscope memory
- Settling time of the positioning system

The lateral and radial search range, and the sampling density, will depend on wavelength, aperture and focus. Even with a judicious choice of operating conditions, the measurement time for a single probe can extend to several days.

II. APPROACH

A. Method and goals

We wish to improve the accuracy, traceability and (if possible) speed of our acoustic power measurements while adhering strictly to the letter and spirit of the 510(k) specification. Our approach has been to:

1. Implement a linear simulator driven by the ultrasound imager's parameters (F-number, focal positions, etc.) This simulator is based on *FIELD II* by Jørgen Jensen [1].
2. Correct the linear predictions using a nonlinear model. A solution of the Burgers equation by Sigve Tjøtta of the University of Bergen was modified for the case of a focused ultrasound beam. Details of how this was done can be found in [6].
3. Investigate how well this compares with measurements using a hydrophone and water tank.
4. Calibrate several unknown parameters to match the experimental data.
5. Model nonlinearities explicitly using, for example, the algorithm developed by Wojcik *et al.* [7].

Thus far, we have tackled items 1-3. The initial goal of this simulation is to prescribe a small volume in which field measurements should take place. The results are validated against the large database of measurements we have accumulated in preparing 510(k) submissions for each revision of the imager. A very conservative standard for acceptance of the simulator's results is obviously appropriate here. Another way to use the simulator is to imagine it as an *intelligent interpolator* which accepts a smaller number of measurements than we usually take, and provides data on a wider selection of discrete operating conditions. In this case, the input data can be thought of as a calibration to set values for poorly defined or simulated parameters. At present, the simulator considers a very wide selection of the operating parameters (e.g., transmit waveform, position of focal zone, F-number, element directivity, etc.)

B. Linear simulation

The linear simulation in *FIELD II* is based on the convolution method (see [1] for details and assumptions.) In this method, the transmitted pressure $p_T(\mathbf{r},\mathbf{t})$ can be expressed as the convolution of the probe's spatial impulse response $h(\mathbf{r},\mathbf{t})$ and the time response of the transducer elements, expressed as a velocity $v(t)$:

$$p_T(\mathbf{r},\mathbf{t}) = \rho_0 \frac{\partial \mathbf{v(t)}}{\partial \mathbf{t}} \star \mathbf{h(r,t)}. \tag{2}$$

This solution makes the mild assumption that the time response and $h(\mathbf{r},\mathbf{t})$ are separable. The spatial impulse response relates the transducer geometry to its acoustic field, and has the form:

$$h(\mathbf{r},\mathbf{t}) = \frac{1}{4\pi}\int_{\mathbf{S'}} \frac{\mathbf{v(x',y')}\boldsymbol{\alpha}(\boldsymbol{\theta})\boldsymbol{\delta}[\mathbf{t}-\mathbf{R/c}-\mathbf{d(x',y')}]}{\mathbf{R}}\mathbf{dS'}. \tag{3}$$

In this equation, $h(t)$ is in units of velocity potential divided by time, $v(x,y)$ is the normal component of the velocity of the surface of the transducer, $d(x,y)$ is the time delay at a given point, θ is the angle between the normal to dS' and the field point, $\alpha(\theta)$ is an inclination factor determined by the boundary condition, and R is the distance from dS' to the field point at $\mathbf{r}$. This integral can be solved analytically for some simple, circularly symmetric, sources.

C. Nonlinear extension

Our nonlinear correction is derived from a solution of the one-dimensional Burgers equation

$$\frac{\partial \overline{p}}{\partial z} = \frac{\beta}{c_0}\overline{p}\frac{\partial \overline{p}}{\partial \tau}, \tag{4}$$

where the depth is z, the nonlinearity parameter is β, c_0 is the speed of sound in the medium, the retarded time $\tau = t - z/c_0$, and the normalized pressure $\overline{p}$ is

$$\overline{p} \triangleq \frac{p - p_0}{\rho_o c_0^2}. \tag{5}$$

Here ρ_o is the density of the medium and p_0 is the ambient pressure (see [6].)

III. RESULTS

A. On-axis derated pulse intensity integral (PII.3)

Figure 1 compares the experimental data with the simulation. The measurements were done with a 0.4 mm diameter hydrophone attached to a motorized positioning system. The data compares a 7 MHz linear probe in B-mode, along the boresight of the probe. That is, the hydrophone is at the center of the aperture in elevation, and at the beam origin in azimuth (the scanning direction). The data begins at Z_B, the *breakpoint* in the range dimension. This range is the definition in the official specification of where near-field effects end. In the graph, measurement points are marked with an $\times$, while a $\square$ indicates a simulated PII.3. It is proportional to the integral of the squared pressure generated by the probe, derated by 0.3 $\mathrm{dB\,cm^{-1}MHz^{-1}}$. The simulation takes account of all of the nuances of the imager's programming, and compares well with measurement. After a point-spread function is computed by *FIELD II*, the pressure is corrected for nonlinear effects.

To gain confidence in the simulator, comparisons were made with a variety of probes, and in all modes the imager supports. Figure 2 shows a comparison for a probe with

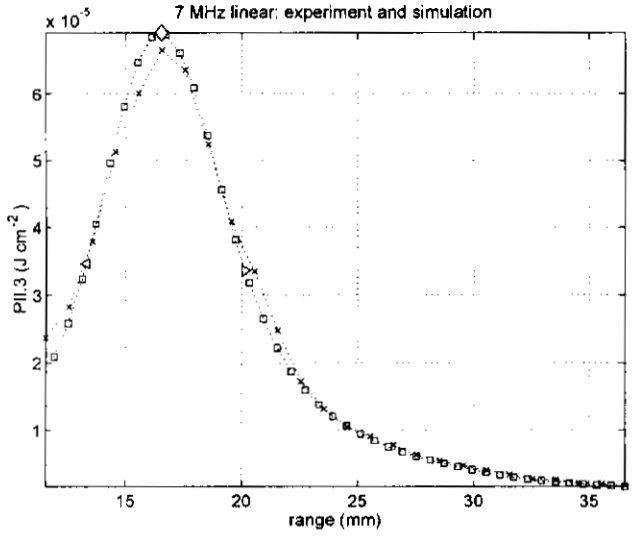

Fig. 1. Comparing the predicted and measured pulse intensity integral (derated: PII.3). The measurements, made in a water tank with a 0.4 mm diameter hydrophone, are plotted using crosses. Predictions are indicated by squares. For this probe and condition, the agreement is very satisfactory.

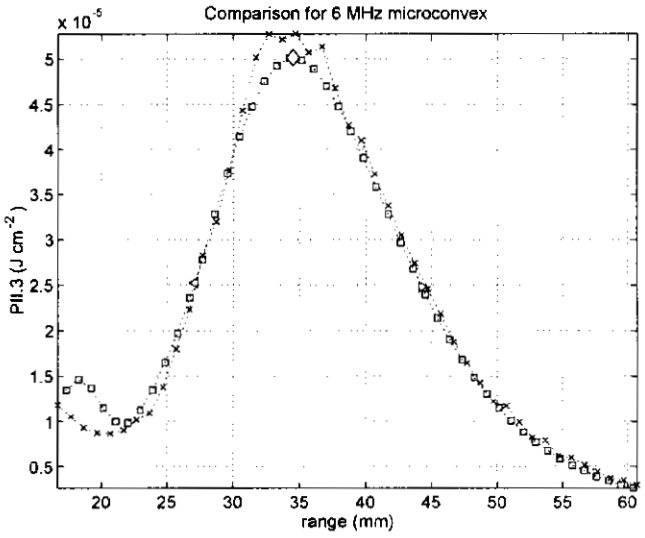

Fig. 2. For the simulation to be useful, it must work for all probes. In this plot we test it for a tightly curved array. The graph symbols are the same as in figure 1.

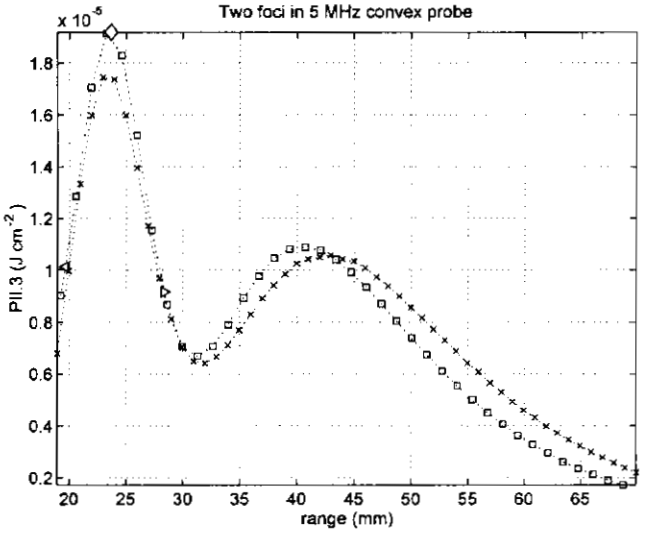

Fig. 3. Another comparison: here the foci from the beamformer and the elevation lens are apparent. In every case, data is shown for the values of azimuth and elevation that maximize acoustic power.

completely different geometry—a 6 MHz micro-convex. Again, the result is encouraging. Figure 3 shows a plot from a 5 MHz convex probe, where neither the beamformer's focus (in azimuth) nor the elevation lens's effect are dominant. In this case, the simulator does not predict the location of the second peak accurately. Section IV speculates about possible causes of this lack of correlation between the model and the measurement. These graphs are useful to compare specific imaging conditions, but we also need an overall view of the technique's effectiveness. A simulation run will generate these data for every setting of the imager that produces a unique acoustic power, in B-mode, Color Flow and Doppler, for dozens of settings of the transmit focal length. The next section describes a way to visualize the accuracy over all the results for a given probe and mode.

B. Overall accuracy of method

One goal of this study is to predict *brackets*, that is, a small subset of the total volume in which to measure the acoustic power. The current simulator's accuracy at this task is shown in figure 4, for a selection of possible focal positions from a 2.5 MHz phased array. The quantity compared is the same as before: the derated pulsed intensity integral. The simulation predicts the correct bracket in every case, when the nonlinear correction is applied (the brackets are denoted by the error bars, and delimited by the -6 dB points of the simulated value.) The actual predicted value is shown by the dots in the figure; and the line is simply $y = x$. If the simulation were perfect, this graph would have all of the simulated values on the line of gradient 1 ($y = x$): then, the model matches the measurement. If the dot deviates significantly from this line, the accuracy is poorer. If the error bar is large, the simulation has had difficulty in identifying the peak. This is not desirable, since we need a high degree of certainty that the computed range subsets always contain the peak.

The sheer quantity of data involved is illustrated in figure 5. This graph shows the results for a 7 MHz linear probe, operated in B-mode. While this large number of data-points requires careful book-keeping, it also allows us to draw statistical conclusions about the accuracy of the simulator.

Figure 6 shows a failure of the algorithm. This is a 10 MHz linear in Color Flow mode. While most of the

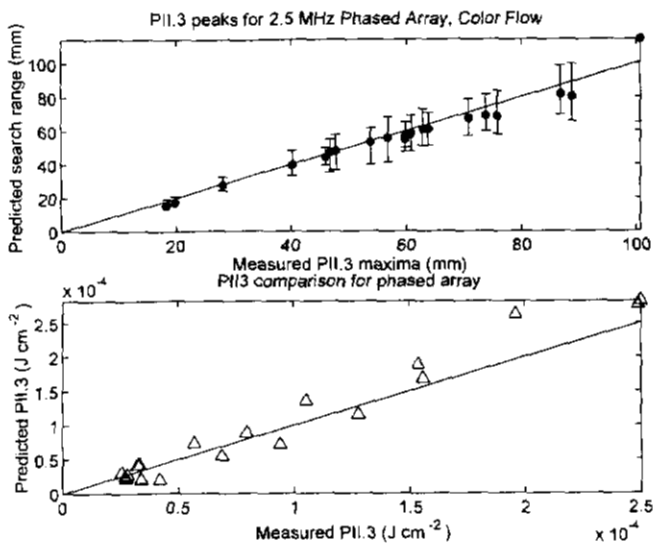

Fig. 4. The upper graph shows how well the simulation predicts a small range to perform a faster measurement of the acoustic power. The dots are the values of the predicted PII.3 maxima. They are plotted against the measured maxima, so they should lie on the diagonal line. The error bars give the simulation -6 dB ranges. The lower graph gives an overview of the accuracy in the estimation of PII.3. Once again, the plot symbols should lie on the diagonal line.

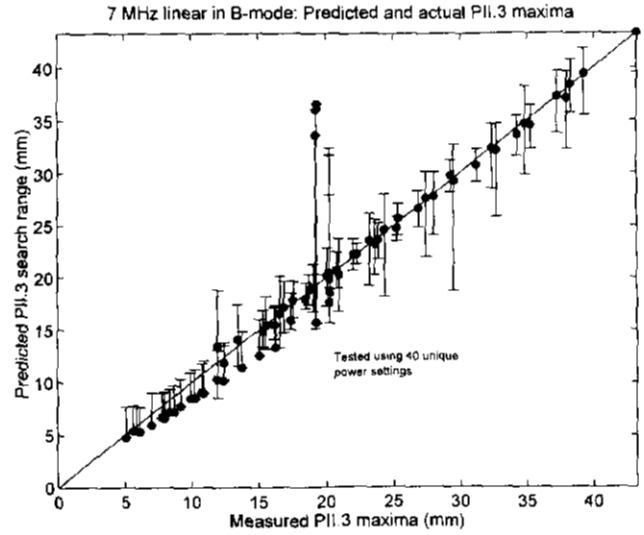

Fig. 5. Our presets produce a large selection of acoustic output levels for each probe. This type of graph gives an overall view of the reliability of the simulation.

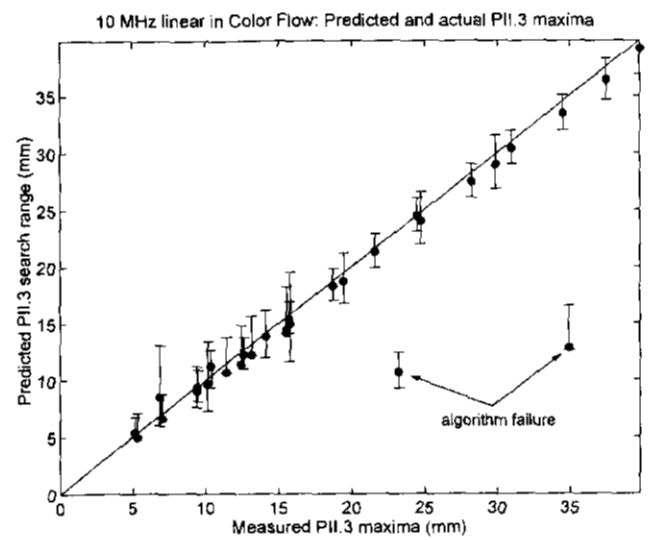

Fig. 6. The simulation's brackets do not always agree with our measurements. The two points far from the diagonal line illustrate this. Either these conditions violate the simulator assumptions too seriously, or the measurement failed.

simulation is acceptable, the two marked points fail badly. At present, we do not know of any correlations between probe dimensions or frequency, and such disagreement in the results. Similar behavior to the results in Figures 1–6 have been seen across several other transducers.

IV. DISCUSSION

The data presented (together with numerous other results not plotted here) inspire confidence that we are presenting correct apertures to the *FIELD II* simulator. Since many of the parameters involved are time- and depth-dependent, this is complex. The predicted brackets are encouraging, but in regulatory acoustic power work, the criterion for success is very strict: we cannot afford to miss *any* peaks if the technique is to be useful. The accuracy of the predicted PII.3 values (rather than the brackets) is less than we would like.

In order to noticeably speed up the verification of a new probe in scanned modes, we need to predict the spatial overlap of successive beams. That quantity, a measure of the amount of the dose delivered from beams pointing in any direction, is needed to derive the scanned intensity integral (SII.3), and the final $I_{\mathrm{SPTA.3}}$. We cannot predict this accurately with a linear simulation: the pressure waveforms we record with the hydrophone show significant shock loss in an appreciable fraction of the cases measured. Since the nonlinear correction [6] assumes weak shock, the loss of accuracy in certain cases is not surprising. A better solution is an explicitly nonlinear model, such as a finite element simulation [7] to provide the needed accuracy for these more challenging tasks.

The effects of phase cancellation on hydrophone readings at focus has not been studied. For high frequency probes, this may affect accuracy. What is measured is the integral over the effective aperture (perhaps 0.5 mm in diameter for our hydrophone), which we are comparing with the pressure at a point. Whether or not this is significant should be investigated.

Another issue is how well we understand the behavior of the real transducer aperture. In the scanning direction, the amplitude and phase across the aperture is well known. In order to produce clinically useful images, these must be tightly controlled. In elevation, the situation is much less

clear. The acoustic lens material is attenuating, and has a convex shape in a typical probe. The lens will therefore tend to make the output from the center of the elevation aperture smaller than at the edges. However, the piezoelectric ceramic may be clamped at its edges by the probe case. This would have the opposite effect on the amplitude profile. The size of each of these effects is unknown, but could be measured by acousto-optic techniques. Another possibility is to estimate the effect by supplying the simulator with measured elevation beam profiles at one or two ranges. These fine corrections are best left until the nonlinear model is complete.

V. CONCLUSIONS

We have constructed a simulation of a real imager that is capable of predicting a small range (10–15% of the normal measurement range) in which to make regulatory measurements of PII.3. In order to expand its usefulness to other acoustic power parameters, we need to improve the nonlinear simulation. Once the simulator is completely validated, other applications become possible. One way of improving our understanding of the statistics of the acoustic output is to run the simulator in a stochastic mode. Tolerances in the transducer and electronics can then be propagated into distributions for $I_{\mathrm{SPTA.3}}$ and MI. Comparing this with our current sampled production test data would provide additional evidence that we have these crucial parameters well controlled. Techniques such as *Fast Probabilistic Integration* [8] can estimate the fraction of the probes which might exceed the regulatory levels with high computational efficiency.

VI. ACKNOWLEDGMENTS

We are very grateful to the people who have assisted in this work. Qian Adams (GEMS Milwaukee) assisted in the data acquisition. Alan Meyers (GEMS Milwaukee) helped with many programming issues. Management at GEMS (Steve Miller) is very supportive of this effort. Jesse Peplinski and Scott Smith (GE-CRD), Kornelija Zgonc (GEMS San Jose), Abraham Bruck (GEMS Israel), Y. Suzuki-san (GE Yokogawa Medical Systems) and Kjell Kristoffersen (GE Vingmed) also contributed helpful insights.

REFERENCES

[1] J.A. Jensen, "A Model for the Propagation and Scattering of Ultrasound in Tissue," *J. Acoust. Soc. Am.* **89**, 182–191 (1991).

[2] National Electrical Manufacturers Association, "Acoustic Output Measurement Standard for Diagnostic Equipment," *NEMA Standard UD-2.*

[3] K. Sandstrom, "Challenges Associated with Characterizing and Predicting Acoustic Fields in Water," *AIUM Workshop on Effects of Nonlinear Propagation on Output Display Indices,* (1998).

[4] T. Christopher and E.L. Carstensen, "Finite Amplitude Distortion and its Relationship to linear derating formulae for diagnostic ultrasound systems," *Ultrasound in Medicine and Biology* **22**(8), 1103–1116 (1996).

[5] E. Madsen, G.R. Frank and F. Dong, "Liquid or solid ultrasonically tissue-mimicking materials with very low scatter ," *Ultrasound in Medicine and Biology* **24**(4), 535-542 (1992).

[6] C.M.W. Daft, W.M. Leue, K.E. Thomenius, L.A. Odegaard, M.C. Macdonald and A.S. Meyers, "Acoustic Intensity Simulations for Regulatory Compliance," in *Medical Imaging 1999: Ultrasonic Transducer Engineering,* K. Kirk Shung, Editor, Proceedings of SPIE Vol. 3664, 212-220 (1999).

[7] G. Wojcik, T. Szabo, J. Mould, L. Carcione, F. Clougherty and I. Sandler, "Nonlinear pulse calculations & data in water and a tissue mimic" in *Proc. IEEE Ultrasonics Symposium, Lake Tahoe, NV* (1999).

[8] Y.-T. Wu, H.R. Millwater and T.A. Cruse, "Advanced Probabilistic Structural Analysis Method for Implicit Performance Functions," *AIAA Journal* **28**(9), 1663–1669 (1992).